*Structural Engineering and Mechanics, Vol. 2, No. 4 (1994) 345-357*
DOI: http://dx.doi.org/10.12989/sem.1994.2.4.345


# Free vibrations of circular arches with variable cross-section

James F. Wilson†

*Department of Civil Engineering, Duke University, Durham, N.C. 27708-0287, U.S.A.*

Byoung Koo Lee† and Sang Jin Oh‡

*Department of Civil Engineering, Wonkwang University, Iri, Junbuk 570-749, Korea*

**Abstract.** The differential equations governing free, in-plane vibrations of linearly elastic circular arches with variable cross-sections are derived and solved numerically for quadratic arches with three types of rectangular cross sections. Frequencies, mode shapes, cross-sectional load distributions, and the effects of rotatory inertia on frequencies are reported. Experimental measurements of frequencies and their corresponding mode shapes agree closely with those predicted by theory. The numerical methods presented here for computing frequencies and mode shapes are efficient and reliable.

**Key words:** circular arch; free vibration; mode shape; quadratic arch; rotatory inertia; variable cross-section.

## 1. Introduction

The governing equations and the significant historical literature on the in-plane vibrations of linearly elastic arches with uniform cross-section are reported in references (Wolf 1971, Veletsos, *et al.* 1972, Romanelli and Laura 1972, Davis, *et al.* 1972, Austin and Veletsos 1973, Wang 1975, Irie, *et al.* 1983, and Lee and Wilson 1990) and their citations. For arches with variable cross-section, Royster (1966) computed the fundamental extensional frequency of a clamped tapered circular arch; Wang (1972) computed the fundamental extensional frequency of a clamped parabolic arch with variable width and depth; and Laura, *et al.* (1988) calculated the fundamental frequency of a circumferential arch with thickness varying in a discontinuous fashion. In the works just cited, the Rayleigh-Ritz method was used. Sakiyama (1985) presented another approximate method for analysing the free vibrations of arches with variable cross-section and non-symmetrical axis.

The main purpose of this paper is to present both the fundamental and some higher free vibration frequencies for linearly elastic circular arches with variable cross-section in which rotatory inertia is included. The differential equations for in-plane vibration are derived and solved numerically.

Numerical results are presented for quadratic arched members of variable cross-section. Three

† Professor
‡ Graduate Student

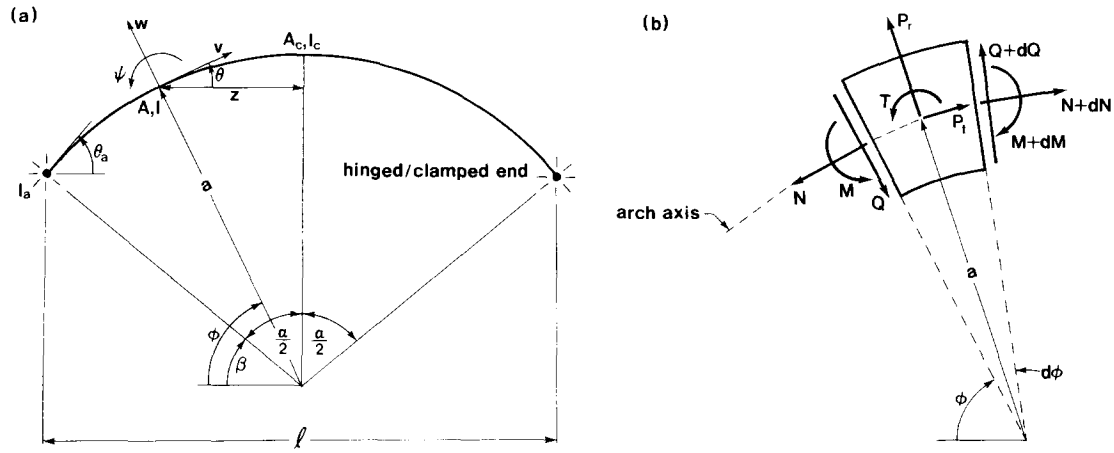


Fig. 1 (a) Arch geometry; (b) Loads on an arch element.

general cross-sectional shapes of rectangular section are selected. Hinged-hinged and clamped-clamped end constraints are considered. The effects of the cross-sectional shapes on the frequencies are reported. The lowest four natural frequencies are presented as functions of three non-dimensional system parameters: (1) the ratio of moment of inertia of cross-section of the end to that of arch crown ratio, (2) the slenderness ratio and (3) the subtended angle. Typical mode shapes of deformations and cross section load distributions are presented. Also included are experimental results that serve to validate the theory.

## 2. Mathematical model

The geometry of the circular arch with variable cross-section, symmetric about the crown, is depicted in Fig. 1(a). Its radius, subtended angle and span length are $a$, $\alpha$ and $l$, respectively. The radial line to a typical arch point is inclined at angle $\phi$ with the horizontal. The left support is at $\phi=\beta$. Shown in Fig. 1(a) are the positive direction of radial and tangential displacements, $w$ and $v$, and positive direction of the rotation angle $\psi$ of the cross section at point $\phi$.

The area moments of inertia of cross-section at $\phi$, at the crown of arch and at the left/right end are denoted as $I$, $I_c$ and $I_a$, respectively. The cross sectional areas at $\phi$ and at the crown of arch are depicted as $A$ and $A_c$. The abscissa $z$ is measured from at any point of arch $\phi$ to the arch vertical center line and the angle between the arch axis and the horizontal is $\theta$. The angle between the arch axis and the horizontal at the left end support is $\theta_a$ which is equal to half the subtended angle, or $\alpha/2$.

The quantities $I$ and $A$ are expressed in the form

$$I=I_cF,\ A=A_cG \tag{1,2}$$

where both $F=F(\phi)$ and $G=G(\phi)$ are the functions of the single variable $\phi$, as discussed in section 3.

A small element of the arch shown in Fig. 1(b) defines the positive directions for its loads: the axial forces $N$; the shear forces $Q$; the bending moments $M$; the radial inertia force $P_r$; the tangential inertia force $P_t$; and rotatory inertia couple $T$. With the inertia forces and the

inertia couple treated as equivalent static quantities, the three equations for "dynamic equilibrium" of the element are

$$dN/d\phi+Q+aP_t=0,\ dQ/d\phi-N+aP_r=0,\ a^{-1}dM/d\phi-Q-T=0 \tag{3-5}$$

The equations that relate $N$, $M$ and $\psi$ to the displacements $w$ and $v$ account for axial deformations due to $N$. These equations, given by Borg and Gennaro (1959), are

$$N=EAa^{-1}(v'+w)+EIa^{-3}(w''+w)=EA_cGa^{-1}(v'+w)+EI_cFa^{-3}(w''+w) \tag{6}$$

$$M=-EIa^{-2}(w''+w)=-EI_cFa^{-2}(w''+w) \tag{7}$$

$$\psi=a^{-1}(w'-v) \tag{8}$$

where each prime is one derivative with respect to $\phi$ and $E$ is Young's modulus.

The arch is assumed to be in harmonic motion, or each coordinate is proportional to $\sin(\omega t)$ where $\omega$ is the frequency parameter and $t$ is time. The inertia loadings per unit arc length are then

$$P_r=\gamma A\omega^2 w=\gamma A_cG\omega^2 w \tag{9}$$

$$P_t=\gamma A\omega^2 v=\gamma A_cG\omega^2 v \tag{10}$$

$$T=\gamma I\omega^2\psi=\gamma I_cF\omega^2a^{-1}(w'-v) \tag{11}$$

where $\gamma$ is mass density of arch material and $\gamma A=\gamma A_cG$ is mass per unit arc length at any point of arch.

When Eqs. (6) and (7) are differentiated once, the results are

$$dN/d\phi=EA_cG'a^{-1}(v'+w)+EA_cGa^{-1}(v''+w')+EI_cF'a^{-3}(w''+w)+EI_cFa^{-3}(w'''+w') \tag{12}$$

$$dM/d\phi=-EI_cF'a^{-2}(w''+w)-EI_cFa^{-2}(w'''+w') \tag{13}$$

When Eqs. (11) and (13) are substituted into Eq. (5), then

$$Q=a^{-1}dM/d\phi-RT=-EI_cF'a^{-3}(w''+w)-EI_cFa^{-3}(w'''+w')-R\gamma I_cF\omega^2a^{-1}(w'-v) \tag{14}$$

Here $R=0$ if rotatory inertia is ignored and $R=1$ if rotatory inertia is included.

The following equation is obtained by differentiating Eq. (14):

$$\begin{aligned} dQ/d\phi=&-EI_cF''a^{-3}(w''+w)-EI_cF'a^{-3}(w'''+w')-EI_cF'a^{-3}(w'''+w')\\ &-EI_cFa^{-3}(w''''+w'')-R\gamma I_cF'\omega^2a^{-1}(w'-v)-R\gamma I_cF\omega^2a^{-1}(w''-v') \end{aligned} \tag{15}$$

To facilitate the numerical studies, the following non-dimensional system variables are defined. The first is the frequency parameter,

$$C_i=\omega_i a^2(\gamma A_c/EI_c)^{1/2} \tag{16}$$

which is written in terms of the $i$th frequency $\omega=\omega_i$, $i=1,2,3,4,\cdots$. The slenderness ratio $s$ is

$$s=a/(I_c/A_c)^{1/2} \tag{17}$$

The displacements are normalized by the arch radius $a$:

$$\xi=w/a,\ \eta=v/a \tag{18a, b}$$

When Eqs. (15), (6) and (9) are substituted into Eq. (4) and the non-dimensional forms of

Eqs. (16)~(18) are used, the result is

$$\xi''''=-2F'F^{-1}\xi'''-(Rs^{-2}C_i^2+F''F^{-1}+2)\xi''+(Rs^{-2}C_i^2-2)F'F^{-1}\xi' +(C_i^2GF^{-1}-F''F^{-1}-s^2GF^{-1}-1)\xi+(Rs^{-2}C_i^2-s^2GF^{-1})\eta' +Rs^{-2}C_i^2F'F^{-1}\eta \tag{19}$$

When Eqs. (12), (14) and (10) are substituted into Eq. (3) and Eqs. (16)~(18) are used, the result is

$$\eta''=(Rs^{-4}C_i^2FG^{-1}-1)\xi'-G'G^{-1}\xi-G'G^{-1}\eta'-s^{-4}C_i^2(RFG^{-1}+s^2)\eta \tag{20}$$

The Eqs. (19) and (20) with $F=G=1$ and $F'=F''=G'=0$ are reduced to governing differential equations for in-plane free vibration of circular arch with the uniform cross-section and these reduced results coincide with equations of Veletsos, *et al.* (1972).

For the hinged-hinged arch, the boundary conditions at the ends $\phi=\beta$ and $\phi=\alpha+\beta$ are

$$\xi=0,\ \eta=0,\ \xi''=0 \tag{21-23}$$

where the last condition assures that the moment $M$ given by Eq. (7) is zero.

For the clamped-clamped arch, the boundary conditions at the ends $\phi=\beta$ and $\phi=\alpha+\beta$ are

$$\xi=0,\ \eta=0,\ \xi'=0 \tag{24-26}$$

where the last condition assures that the end rotation $\psi$ given by Eq. (8) is zero.

Arch stresses may be computed from the following nondimensional forms for the bending moment $M$, the normal load $N$, and the transverse shear load $Q$. The respective results, obtained from Eqs. (7), (6) and (14) using Eqs. (16)-(18), are:

$$m=Ma/EI_c=-F(\xi''+\xi) \tag{27}$$

$$n=Na^2/EI_c=s^2G(\eta'+\xi)+F(\xi''+\xi) \tag{28}$$

$$q=Qa^2/EI_c=-F'(\xi''+\xi)-F(\xi'''+\xi')-Rs^{-2}C_i^2F(\xi'-\eta) \tag{29}$$

## 3. Shape functions: *F* and *G*

The shape functions $F$ and $G$ first introduced in Eqs. (1) and (2), and contained in the governing differential Eqs. (19) and (20), are now defined. Of the two basic classes of arched members, prime and quadratic (Leontovich 1969), the quadratic arch is considered here. Examples are also limited rectangular cross sections.

First, the function $F$ is derived for the quadratic arch. A quadratic arch is defined as an arch whose moment of inertia of cross-section varies in accordance with the quadratic equation:

$$I=\frac{I_c}{\left\{1-\left[1-\frac{I_c}{I_a\cos\theta_a}\right]\left[\frac{2z}{l}\right]^2\right\}\cos\theta} \tag{30}$$

The terms of $\theta$ and $z/l$ in above equation can be expressed in the variable $\phi$ as follows.

$$\theta=\pi/2-\phi,\ 2z/l=\mathrm{cosec}(\alpha/2)\cos\phi \tag{31,32}$$

A new non-dimensional parameter is defined as the ratio of $I_a$ and $I_c$:

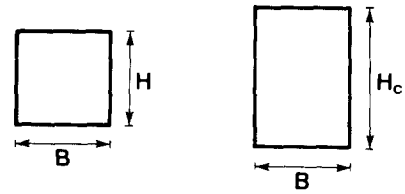


**(a) depth taper: constant width and variable depth**

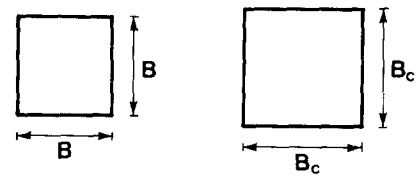


**(b) square taper: square cross section**

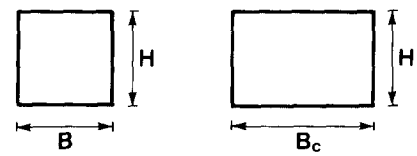


**(c) breadth taper: variable width and constant depth**

Fig. 2 Cross-sectional shapes.

$$k=I_a/I_c \tag{33}$$

When Eqs. (31)~(33) and $\theta_a=\alpha/2$ are substituted into Eq. (30), the result is

$$I=I_c\,\mathrm{cosec}\phi/(1+D\cos^2\phi) \tag{34}$$

where

$$D=\mathrm{cosec}^2(\alpha/2)\left[\frac{\sec(\alpha/2)}{k}-1\right] \tag{35}$$

When Eqs. (1) and (34) are combined, the function of $F$ can be expressed in terms of the variable $\phi$. The result is

$$F=\mathrm{cosec}\phi/(1+D\cos^2\phi) \tag{36}$$

When Eq. (36) are differentiated once and twice, the results are

$$F'=F^2\cos\phi(-3D\cos^2\phi+2D-1) \tag{37}$$

$$F''=2F^{-1}F'^2+F^2\sin\phi(9D\cos^2\phi-2D+1) \tag{38}$$

Second, the function $G$ is defined for the following three rectangular cross sections.

(a) Depth taper, Fig. 2(a). The beam width of $B$ is constant, and the beam depth at any point of arch is denoted as $H$ and at crown as $H_c$. With the relations of $I_c=BH_c^3/12$ and $I=BH^3/12$, the following result is obtained using Eq. (1).

$$I=\frac{BH_c^3}{12}F=\frac{BH^3}{12} \tag{39}$$

Using Eq. (39), the variable depth $H$ is expressed as

$$H=H_cF^{1/3} \tag{40}$$

With the relations $A_c=BH_c$, $A=BH$, and Eq. (40), then the area becomes

$$A=BH=BH_cF^{1/3}=A_cF^{1/3} \tag{41}$$

With Eqs. (2) and (41), $G$ is expressed in terms of $F$ as

$$G=F^{1/3} \tag{42}$$

When Eq. (42) is differentiated once, then the result is

$$G'=F^{-2/3}F'/3 \tag{43}$$

(b) Square taper, Fig. 2(b). This is the square cross-section so the beam width and depth at any point of arch are equal. With the derived as same procedure as in (a), the functions $G$ and $G'$ are functions of $F$ and $F'$, or

$$G=F^{1/2}, \qquad G'=F^{-1/2}F'/2 \tag{44, 45}$$

(c) Breadth taper, Fig. 2(c). The functions $G$ and $G'$ are expressed as

$$G=F, \qquad G'=F' \tag{46, 47}$$

The theoretical results are summarized. The governing differential Eqs. (19) and (20) for the in-plane free vibration displacement mode shapes ($\xi$, $\eta$) form a sixth order system. When subject to the six homogeneous boundary conditions (three on each end of the arch), given by either Eqs. (21)~(23) for the hinged-hinged arch, or by Eqs. (24)~(26) for the clamped-clamped arch, the $i$th frequency parameter (eigenvalue) $C_i$ and its corresponding mode shapes (eigenfunctions) $\xi=\xi_i$ and $\eta=\eta_i$ may be computed from the governing Eqs. (19) and (20). To compute these solutions, one must specify the following arch parameters that appear in these governing equations: the arch angle $\alpha$; slenderness ratio s of Eq. (17); the geometric ratio $k$ of Eq. (33); the rotatory inertia where $R=1$ if included and $R=0$ if ignored; and the cross sectional shape factors $F$ and $G$. For the quadratic arch defined by Eq. (30), with $\alpha$ and $k$ specified, then $D$, $F$ and the derivatives of $F$ are computed from Eqs. (35)~(38). For a rectangular cross section with a taper chosen from either type (a), (b), or (c), then the values of $G$ and $G'$ are given by Eqs. (42), (43), or (44), (45), or (46), (47), respectively. With solutions to the governing equations, the three cross sectional load distributions, the bending moment $m=m_i$, the normal load $n=n_i$, and the transverse shear load $q=q_i$, are then computed from Eqs. (27)~(29), respectively. Numerical results are now illustrated.

## 4. Numerical method and computed results

Based on the above analysis, a general FORTRAN computer program was written to calculate $C_i$, $\xi=\xi_i(\phi)$, $\eta=\eta_i(\phi)$, $m=m_i(\phi)$, $n=n_i(\phi)$ and $q=q_i(\phi)$. The numerical method described by Veletsos, *et al.* (1972) was used to solve the differential Eqs. (19) and (20), subject to the end constraint Eqs. (21)~(23) or (24)~(26). The hinged-hinged and clamped-clamped end constraints were consi-

Table 1 Comparison of frequency parameter $C_i$ between this study and finite element method (SAP 90)

| Geometry of arch | | $i$ | Frequency parameter, $C_i$ | |
|---|---|---|---|---|
| | | | This study ($R=1$) | SAP 90 |
| Hinged ends and square taper | $\alpha=90°$ $s=100$ $k=0.5$ | 1 | 12.38 | 12.40 |
| | | 2 | 28.52 | 28.61 |
| | | 3 | 56.18 | 56.36 |
| | | 4 | 82.56 | 82.76 |
| | $\alpha=90°$ $s=100$ $k=3$ | 1 | 14.81 | 14.80 |
| | | 2 | 35.73 | 35.70 |
| | | 3 | 66.98 | 67.09 |
| | | 4 | 93.41 | 93.45 |
| Clamped ends and square taper | $\alpha=90°$ $s=100$ $k=0.5$ | 1 | 19.72 | 19.75 |
| | | 2 | 36.84 | 36.95 |
| | | 3 | 70.56 | 70.80 |
| | | 4 | 85.98 | 86.09 |
| | $\alpha=90°$ $s=100$ $k=3$ | 1 | 27.12 | 27.08 |
| | | 2 | 48.79 | 48.75 |
| | | 3 | 87.87 | 88.02 |
| | | 4 | 93.55 | 93.59 |

Table 2 Effect of rotatory inertia on frequency parameter $C_i$

| Geometry of arch | Cross sectional shapes | $R$ | Frequency parameter, $C_i$ | | | |
|---|---|---|---|---|---|---|
| | | | $i=1$ | $i=2$ | $i=3$ | $i=4$ |
| Hinged ends $\alpha=90°$, $s=100$ $k=3$ | Depth taper | 0 | 15.15 | 36.40 | 68.91 | 93.14 |
| | | 1 | 15.13 | 36.33 | 68.65 | 93.02 |
| | Square taper | 0 | 14.82 | 35.80 | 67.22 | 93.54 |
| | | 1 | 14.81 | 35.73 | 66.98 | 93.41 |
| | Breadth taper | 0 | 13.83 | 33.78 | 62.20 | 93.41 |
| | | 1 | 13.82 | 33.72 | 62.00 | 93.19 |
| Clamped ends $\alpha=90°$, $s=100$ $k=3$ | Depth taper | 0 | 27.57 | 49.25 | 90.15 | 93.16 |
| | | 1 | 27.54 | 49.16 | 89.79 | 93.04 |
| | Square taper | 0 | 27.15 | 48.88 | 88.21 | 93.65 |
| | | 1 | 27.12 | 48.79 | 87.87 | 93.55 |
| | Breadth taper | 0 | 25.87 | 47.39 | 82.35 | 94.91 |
| | | 1 | 25.85 | 47.32 | 82.07 | 94.82 |

dered for the three cross-sectional shapes, for given parameters $\alpha$, $s$, $k$ and $R(=0$ or 1). First, the Determinant Search Method was used to calculate the characteristic values $C_i$; and then the Runge-Kutta method was used to calculate the mode shapes. In this study, the four lowest values of $C_i$ and the corresponding mode shapes were calculated. The numerical results, given in Tables 1~3 and Figs. 3~6, are summarized as follows.

In Table 1, values of $C_i$ are presented for square, tapered arches with clamped and hinged

Table 3 Effect of cross-sectional shapes on frequency parameter $C_i$

| Geometry of arch | $k$ | Cross sectional shape | Frequency parameter, $C_i$ | | | |
|---|---|---|---|---|---|---|
| | | | $i=1$ | $i=2$ | $i=3$ | $i=4$ |
| Hinged ends $\alpha=90°$ $s=100$ $R=1$ | 0.5 | Depth taper | 12.06 | 28.06 | 54.64 | 82.28 |
| | | Square taper | 12.38 | 28.52 | 56.18 | 82.56 |
| | | Breadth taper | 13.34 | 29.74 | 60.91 | 85.17 |
| | 3.0 | Depth taper | 15.13 | 36.33 | 68.65 | 93.02 |
| | | Square taper | 14.81 | 35.73 | 66.98 | 93.41 |
| | | Breadth taper | 13.82 | 33.72 | 62.00 | 93.19 |
| Clamped ends $\alpha=90°$ $s=100$ $R=1$ | 0.5 | Depth taper | 19.29 | 36.43 | 68.73 | 85.75 |
| | | Square taper | 19.72 | 36.84 | 70.56 | 85.98 |
| | | Breadth taper | 21.02 | 37.80 | 76.13 | 86.26 |
| | 3.0 | Depth taper | 27.54 | 49.16 | 89.79 | 93.05 |
| | | Square taper | 27.12 | 48.79 | 87.87 | 93.55 |
| | | Breadth taper | 25.85 | 47.31 | 82.07 | 94.82 |

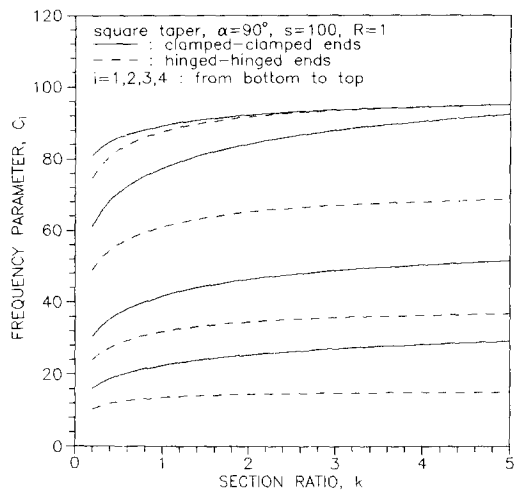


Fig. 3 Effect of section ratio $k$ with $\alpha=90°$, $s=100$, $R=1$ on frequency parameter $C_i$ for square taper.

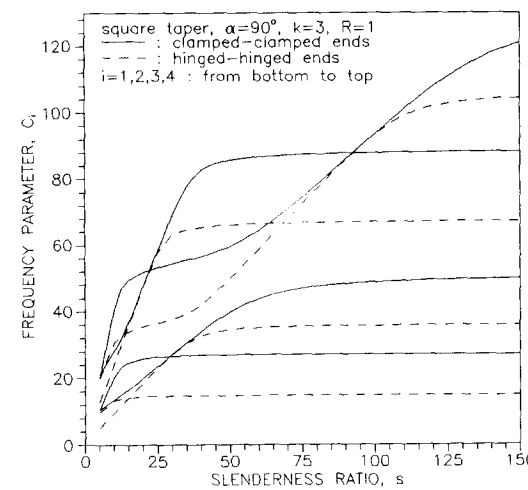


Fig. 4 Effect of slenderness ratio s with $\alpha=90°$, $k=3$, $R=1$ on frequency parameter $C_i$ for square taper.

ends. Comparisons are made between $C_i$ computed using the present analysis with $R=1$ and $C_i$ computed with the packaged finite element program SAP90. For the latter calculations, 100 beam elements were used and effects of shear area were not included. Comparing the results for like arch parameters, the results for $C_i$ agree to within 1%. The remainder of the numerical results are based on the present analysis.

In Table 2 are given the lowest four frequency parameters for all three types of rectangular tapers. For a given geometry, the effects of end restraint and rotatory inertia are apparent: the higher the end restraint, the higher is $C_i$; and the inclusion of rotatory inertia depresses $C_i$ by

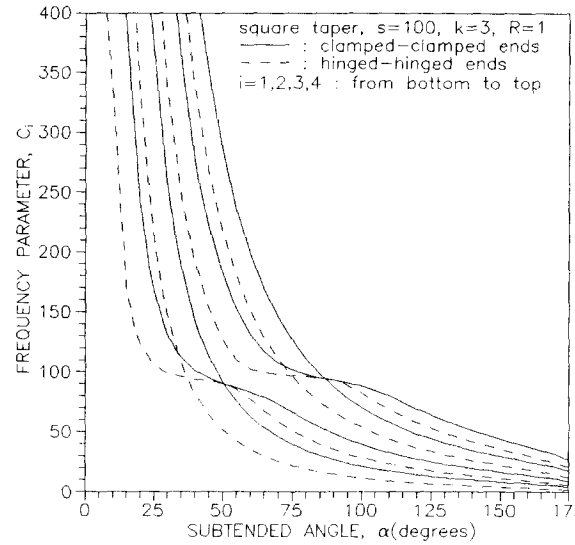


Fig. 5 Effect of subtended angle $\alpha$ with $s=100$, $k=3$, $R=1$ on frequency parameter $C_i$ for square taper.

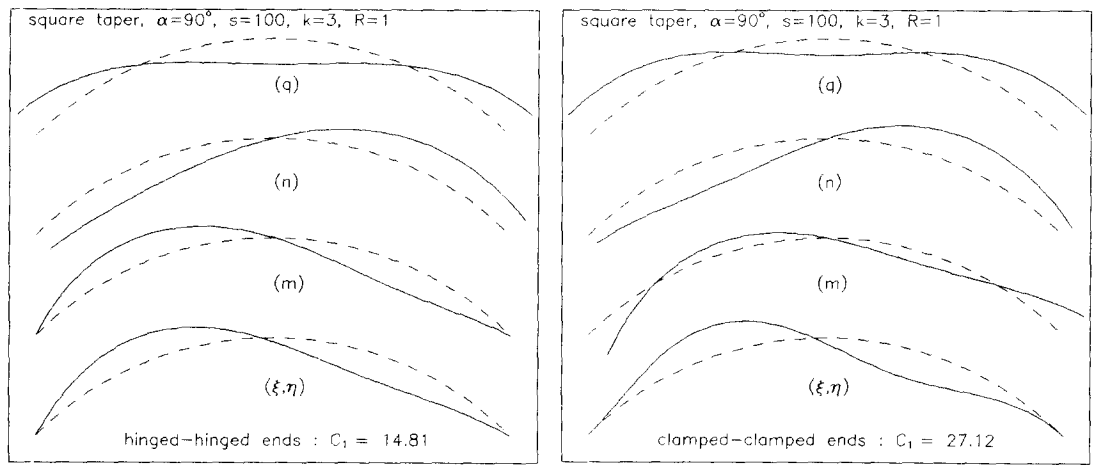


Fig. 6 Fundamental mode shapes of displacements ($\xi$, $\eta$) and cross sectional load distributions ($m$, $n$, $q$) with $\alpha=90°$, $s=100$, $k=3$, $R=1$ for square taper.

less than 1%. A comparison of the results in columns $i=1,2,3$ show that $C_i$ decreases as the type of taper changes from the depth to the square to the breadth taper; but this trend is reversed for $i=4$.

In Table 3, the effects of cross sectional shape on $C_i$ are displayed. Here, $C_i$ always increases as $k$ increases, other parameters remaining the same.

The results shown in Figs. 3~5, all for the square cross section with $R=1$, depict the variation of $C_i$ ($i=1,2,3,4$) with $k$, with $s$, and with $\alpha$, respectively. In Fig. 3, $s=100$, $\alpha=90$ deg and the $C_i$ values approach upper limits or horizontal asymptotes as $k$ increases to 5. In Fig. 4, $k=3$, $\alpha=90$ deg, and the $C_i$ again approach horizontal asymptotes as $s$ increases to 150. In Fig. 5, $k=3$, $s=100$, and the $C_i$ values all decreases very rapidly $\alpha$ increases from 25 deg to 100 deg.

Typical fundamental mode shapes are shown in Fig. 6, based on the square cross section with $R=1$, $k=3$, $s=100$, and $\alpha=90$ deg. For a given end constraint (hinged or clamped), the $(\xi, \eta)$ deflection modes for $C_1$ have the same shape and are asymmetric about the broken line that represents the static equilibrium state. Also shown in Fig. 6 are the cross sectional load distribution mode shapes for moment $m$, for the normal load $n$, and for the transverse shear load $q$, all for $i=1$. In all cases, the accompanying broken lines refer to zero load. As one would expect, when one compares the hinged and clamped configurations, the respective shapes for these loads are about the same except near the ends where $m$ is zero for the hinged end case and non-zero for the clamped end case.

## 5. Experimental results

Experiments were designed to measure the lowest few free vibration frequencies on two aluminum, laboratory-scale circular, tapered arches, one with hinged ends and the other clamped ends. These two arches had the same geometry: quadratic arches described by Eq. (30), with type (c) or breadth taper given by Eqs. (46) and (47). The dimensions, defined in Fig. 1(a) and 2, were: $a=25.5$ cm, $B_c=1.27$ cm, $H=0.635$ cm, and $\alpha=90$ deg, for which the corresponding nondimensional parameters were: $k=2$ and $s=139$. Based on the methods described above in which rotatory inertia was included ($R=1$), the frequency parameters $C_i$ were calculated. The corresponding frequencies $\omega_i$ (rad/s) were computed from Eq. (16) based on the following material properties for the aluminum arches: a Young's modulus $E$ of $6.89\times10^{10}$ N/m$^2$ and a mass density $\gamma$ of 2680 kg/m$^3$. The resulting frequencies $f_i=\omega_i/(2\pi)$ $Hz$, $i=1,2,3,4$ are given in Table 4 for each of the two arches tested.

The experimental setup and methods of measuring the free vibration frequencies of these two arches is fully described by the authors (Lee and Wilson 1990). For the sake of completeness, these methods are now summarized. At each end, the arch was either hinged or clamped to a 50 kg, isolated concrete block where each block "floated" on a rubber pad. Including the end points, 17 reference points spaced along the arch circumference were used. To one of these reference points on the underside of the arch was affixed a miniature accelerometer mounted so that it was sensitive only to radial arch acceleration. In a typical experiment, a hammer also fitted with a miniature accelerometer was struck at each of the reference points, in-plane and in the radial direction of the arch. All acceleration data were received by a Signal Analyzer (Model SD380Z, Scientific-Atlanta Corp.) and processed through a minicomputer using a fast Fourier transform (FFT) analyser. For the details of data reduction, see Ewins (1985).

The data analysis lead to two important results: (1) the frequency dependent Transfer Function defined as the ratio of the magnitude of the FFT for arch acceleration to the magnitude of the FFT for the hammer acceleration; and (2) the radial displacement mode shapes for the arch at the peaks of the Transfer Function. Such a Transfer Function measured for the clamped-clamped arch is illustrated in Fig. 7. The consecutive major peaks of this plot indicate the consecutive free vibration frequencies of this arch, or $f_1=500$ Hz, $f_2=890$ Hz, etc., which are also listed in Table 4. For each of these first four frequencies, the corresponding radial displacement mode shapes generated from measurements are depicted in Fig. 8. These have the same number of node points and have approximately the same shape as $(\xi, \eta)$ computed (but not shown) from the theoretical model at the same respective frequencies. In reality, these measured shapes are smooth and, relative to the undeformed shape shown as the dashed line, have zero slope at each end. However, the software available simply connected data from the 17 reference

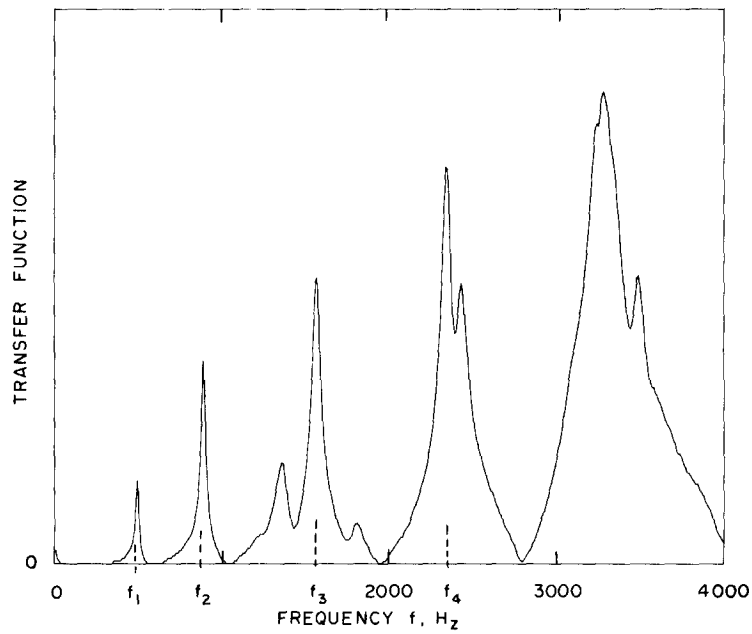


Fig. 7 Transfer function of acceleration for the clamped-clamped experimental arch.

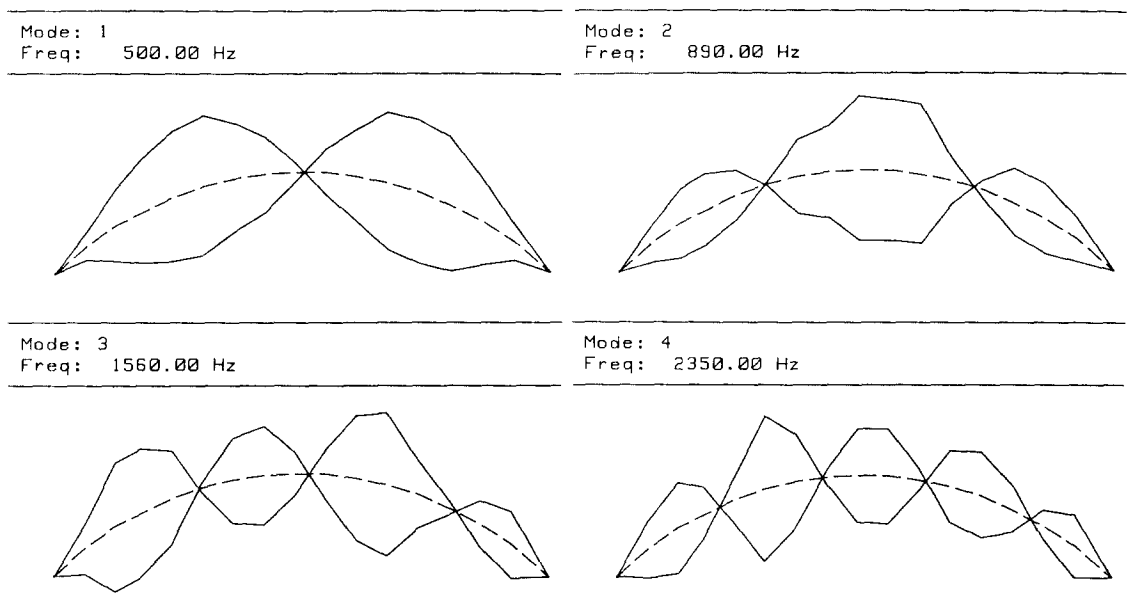


Fig. 8 Measured mode shapes of the clamped-clamped experimental arch.

points with straight lines and thus gave only a crude picture of the theoretical shapes. For the hinged-hinged experimental arch, results similar to those of Fig. 7 and 8 were also obtained, and the resulting frequencies are listed in Table 4.

Considering all of these data, the measured frequencies averaged about 14% less than those predicted from theory. The differences between theory and experiment are of the same order

Table 4 Comparison of computed and measured results (breadth taper, $\alpha=90°$, $s=139$, $k=2$, $R=1$)

| End constraint | Mode no. | Theory | | Experiment | % Deviation experiment from theory |
|---|---|---|---|---|---|
| | | $C_i$ | $f_i$(Hz) | $f_i$(Hz) | |
| Hinged ends | 1 | 13.85(A)* | 315.89 | 285 | −9.8 |
| | 2 | 33.39(S) | 761.57 | 640 | −15.9 |
| | 3 | 61.93(A) | 1412.80 | 1085 | −23.2 |
| | 4 | 96.34(S) | 2197.76 | − | − |
| Clamped ends | 1 | 24.57(A) | 560.55 | 500 | −10.8 |
| | 2 | 45.92(S) | 1047.42 | 890 | −15.0 |
| | 3 | 80.53(A) | 1837.12 | 1560 | −15.1 |
| | 4 | 112.36(S) | 2562.96 | 2350 | −8.3 |

*A: anti-symmetric mode, S: symmetric mode

as obtained on other arch geometries (Lee and Wilson 1990) and may be accounted for by several factors: the experimental difficulties of achieving "perfect" hammer strikes exactly on the arch centerline, where imperfect hammer strikes led to out-of-plane free vibrations; difficulties of achieving the ideal end constraint conditions (clamped or hinged); and the presence of natural structural damping in the experiments which was not included in the theoretical model.

## 6. Conclusions

The methods presented here for calculating frequencies and mode shapes for circular, quadratic arches of variable cross section were found to be efficient and reliable over a wide range of system parameters. Computations showed that rotatory inertia depressed the frequency parameters $C_i$ by less than one percent for such arches with hinged ends and with clamped ends. Results also showed that the type of taper for the quadratic arch (depth, square, or breadth taper) caused variations in $C_i$ by less than one percent, all other parameters remaining the same. For the square taper, the effects of each of the three parameters $k$, $s$ and $\alpha$ on $C_i$ ($i=1,2,3,4$) were investigated for the first time, as were the internal circumferential load distributions of bending moment, normal load, and transverse shear load. Experiments in which frequencies and mode shapes were measured on two breadth-tapered quadratic circular arches, one clamped-clamped and the other hinged-hinged, served to validate the results of the theoretical analysis.

## Acknowledgements

The authors thank Mrinmay Biswas for the use of his experimental modal analyzer system and Arun Pandey for his able assistance with the experiments.

## References

Austin, W. J. and Veletsos, A. S. (1973), "Free vibration of arches flexible in shear", *Journal of the*

*Engineering Mechanics Division, ASCE,* **99**(EM4), 735-753.
Borg, S. F. and Gennaro, J. J. (1959), *Advanced Structural Analysis,* Van Nostrand, New Jersey.
Davis, R., Henshell, R. D. and Warburton, G. B. (1972), "Constant curvature beam finite elements for in-plane vibration", *Journal of Sound and Vibration,* **25**, 561-576.
Ewins, D. J. (1985), Modal Testing: *Theory and Practice,* John Wiley, New York.
Irie, T., Yamada, G. and Tanaka, K. (1983), "Natural frequencies of in-plane vibration of arcs", *Journal of Applied Mechanics, ASME,* **50**, 449-452.
Laura, P. A. A. and Verniere de Irassar, P. L. (1988), "A note on vibrations of a circumferential arch with thickness varying in a discontinuous fashion", *Journal of Sound and Vibration,* **120**(1), 95-105.
Lee, B. K. and Wilson, J. F. (1990), "Free vibrations of arches with variable curvature", *Journal of Sound and Vibration,* **136**(1), 75-89.
Leontovich, V. (1969), *Frames and Arches,* McGraw-Hill.
Romanelli, E. and Laura, P. A. A. (1972), "Fundamental frequencies of non-circular, elastic, hinged arcs", *Journal of Sound and Vibration,* **24**, 17-22.
Royster, L. H. (1966), "Effect of linear taper on the lowest natural extensional frequency of elastic arcs", *Journal of the Applied Mechanics, ASME,* **33**, 2111-2112.
Sakiyama, T. (1985), "Free vibration of arches with variable cross section and non-symmetric axis", *Journal of Sound and Vibration,* **102**, 448-452.
Veletsos, A. S., Austin, W. J., Pereira, C. A. L. and Wung, S. J. (1972), "Free in-plane vibration of circular arches", *Journal of the Engineering Mechanics Division, ASCE,* **98**(EM2), 311-329.
Wang, T. M. (1972), "Lowest natural frequency of clamped parabolic arc", *Journal of the Structural Division, ASCE,* **98**(ST1), 407-411.
Wang, T. M. (1975), "Effect of variable curvature on fundamental frequency of clamped parabolic arcs", *Journal of Sound and Vibration,* **41**, 247-251.
Wolf, J. A., Jr. (1971), "Natural frequencies of circular arches", *Journal of the Structural Division, ASCE,* **97**(ST9), 2337-2350.